Published in final edited form as:

Proteins. 2014 December ; 82(12): 3490–3496. doi:10.1002/prot.24701.

The solution structure of the forkhead box-O DNA binding domain of *Brugia malayi* DAF-16a:

The FOXO domain of *B. malayi* DAF-16a

Sarah K. Casper[1,2,^], **Scott J. Schoeller**[3,^], **Danielle M. Zgoba**[1], **Andrew J. Phillips**[3], **Thomas J. Morien**[3], **Gary R. Chaffee**[3], **Peter C. Sackett**[1,#], **Francis C. Peterson**[4], **Kirsten Crossgrove**[1,*], and **Christopher T. Veldkamp**[3,4,*]

[1]Department of Biological Sciences, University of Wisconsin-Whitewater, 800 West Main Street, Whitewater, WI 53190

[2]Department of Health Sciences, Blackhawk Technical College, 1740 U.S. 41, Janesville, WI 53545

[3]Department of Chemistry, University of Wisconsin-Whitewater, 800 West Main Street, Whitewater, WI 53190

[4]Department of Biochemistry, Medical College of Wisconsin, 8701 Watertown Plank Road, Milwaukee, WI 53226

Abstract

Brugia malayi is a parasitic nematode that causes lymphatic filariasis in humans. Here the solution structure of the forkhead DNA binding domain of *Brugia malayi* DAF-16a, a putative ortholog of *Caenorhabditis elegans* DAF-16, is reported. It is believed to be the first structure of a forkhead or winged helix domain from an invertebrate. *C. elegans* DAF-16 is involved in the insulin/IGF-I signaling pathway and helps control metabolism, longevity, and development. Conservation of sequence and structure with human FOXO proteins suggest that *B. malayi* DAF-16a is a member of the FOXO family of forkhead proteins.

Keywords

Brugia malayi; forkhead box; winged helix; FOXO; FOXO1; FOXO3a; FOXO4; DAF-16; *Caenorhabdtis elegans*; insulin-signaling pathway; filariasis

Introduction

Filarial parasites are nematodes that cause debilitating disease in humans and domestic animals. The human parasite *Brugia malayi* is transmitted by mosquitoes and is one of the causative agents of lymphatic filariasis. According to the Centers for Disease Control and

*Corresponding authors: Christopher T. Veldkamp, Department of Chemistry, University of Wisconsin-Whitewater, 800 West Main Street, Whitewater, WI 53190, veldkamc@uww.edu, Kirsten Crossgrove, Department of Biological Sciences, University of Wisconsin-Whitewater, 800 West Main Street, Whitewater, WI 53190, crossgrk@uww.edu.

#Current Address: Evonik Industries, 900 S Palm St, Janesville, WI 53548.

^These authors contributed equally.

Prevention, transmittance of infective stage (third stage, iL3) larvae from mosquitoes to a human host triggers a molt to the fourth larval stage (L4)[1]. Following a final molt, adult males and females accumulate in the lymphatic system. Disease symptoms are caused primarily by the body's immune response against the parasites and their *Wolbachia* endosymbionts[2]. The Global Programme for the Elimination of Lymphatic Filariasis has made impressive strides towards breaking the transmission cycle through mass drug administration with ivermectin, albendazole and diethylcarbamzine[3]. However, evidence of drug resistance is beginning to emerge[4]. Understanding the development of the parasite, particularly what controls the iL3 to L4 molt when the infective stage first enters the human host, may lead to drug or vaccine targets.

The iL3 stage in parasitic nematodes is considered to be analogous to the dauer developmental stage in the well-studied free-living nematode *Caenorhabditis elegans*[5]. In harsh conditions (lack of food, high temperature, high crowding), *C. elegans* enter the dauer stage, an alternative to the normal third larval stage[6]. Dauer larvae have a thick, highly resistant cuticle, they do not feed, and their metabolism is altered to allow them to remain in stasis until an environmental signal triggers resumption of normal development (molting to the L4 stage)[6]. In addition to both being third stage larvae, both iL3 and dauer also require an environmental signal in order to molt[5]. Several signaling pathways are known to regulate the dauer decision, including an insulin-signaling pathway[7]. Specifically, *Ce*DAF-16 proteins are phosphorylated by AKT and SGK-1 kinases when insulin signaling is active[7]. When phosphorylated, *Ce*DAF-16 binds to the 14-3-3 protein FTT-2 and is localized to the cytoplasm[7]. Unphosphorylated *Ce*DAF-16 is active and localized to the nucleus where it regulates target genes through binding to forkhead response elements (FREs). *Ce*DAF-16 is active during dauer formation and is inactivated by insulin signaling during dauer recovery. Parasitic nematodes may also use the insulin-signaling pathway to molt from the infective stage to the L4 stage on entry into a mammalian host. For example, the *Ancylostoma caninium* DAF-16 and *Strongyloides stercoralis* FKTF-1 (DAF-16) were able to rescue *daf-16* mutant phenotypes in *C. elegans*[8,9] and a dominant negative form of FKTF-1 disrupted morphogenesis of infective stage larvae[10].

A putative *daf*-16 ortholog exists in *B. malayi*. *Bm-daf-16* encodes at least two isoforms, *Bm-daf-16a* and *Bm-daf-16b*, which are alternatively spliced at the 5' end. Deep sequencing[11] and quantitative Real Time PCR (Garland, B. and Crossgrove, K., unpublished) show that *Bm-daf*-16 is expressed in all life cycle stages tested (adults, microfilaria, iL3 and L4), though isoform specific assays have not been conducted. The DNA binding domain encoded by *Bm-daf-16a* exhibits 81% amino acid identity to the *C. elegans* DAF-16a protein, while the *Bm-daf-16b* DNA binding domain is 92% identical to *C. elegans* DAF-16b. While the two *Bm-daf-16* isoforms, and their homologous *C. elegans* isoforms, differ at the N-terminus of the DNA binding domain, they share the predicted DNA recognition helix and are predicted to form functional forkhead domains. NMR and X-ray crystallography studies of forkhead box domain containing proteins, like human forkhead box-O (FOXO) proteins FOXO1, FOXO3a and FOXO4, have demonstrated each has the conserved winged helix or forkhead box DNA binding domain structure containing three to four α-helicies, a three stranded β-sheet and two unstructured wings[12]. Human

FOXO proteins have been intensely studied due to their therapeutic potential[13]. However, to date no structural studies have been done on invertebrate FOXO proteins. Here we describe the solution structure of residues 342-442 of *Bm*-DAF-16a (Uniprot ID A8QCW6) and show that it forms a canonical forkhead box-O DNA binding domain.

Materials and Methods

Undergraduates, as a part of independent research courses, completed the majority of this work.

Protein purification

DNA coding for an SMT3-*Bm*-DAF-16a (residues 342-442) fusion protein was cloned into the Bam-HI and Hind-III sites of pQE30. The UniProt ID for *Bm*-DAF-16a is A8QCW6. Protein was expressed in *Escherichia coli* strain SG13009 containing pLacIRARE for expression of LacI and expression of tRNAs for overcoming codon bias. Cells were grown at 37°C in 1L of Luria broth or [U-^{15}N/^{13}C] M9 minimal medium to an OD600 of 0.6, at which time expression was induced with 1 mM isopropyl β-D-1-thiogalactopyranoside. After 5 hours, cell pellets were collected by centrifugation (4,000 × *g* for 30 min) and stored at −20°C until processing. Cells were resuspended and lysed by sonication in Buffer A (50 mM sodium phosphate, 300 mM NaCl, 10mM imidazole, pH 8.0) containing 0.1% (v/v) β-mercaptoethanol and 1 mM phenylmethanylsulfonyl fluoride. The insoluble protein inclusion body containing His6-SMT3-*Bm*-DAF-16a (342-442) was collected by centrifugation (15,000 × *g* for 15 min) and dissolved in buffer AD (6 M guanidine HCl, 50 mM sodium phosphate, 300 mM NaCl, 10 mM imidazole, 0.1% (v/v) 2-mercaptoethanol, pH 8.0). After clarification by centrifugation (15,000 × *g* for 15 min), the supernatant was loaded onto ~2 mL of His60 nickel resin for 30 min. The column was washed with 40 mL buffer AD. The His6-SMT3-*Bm*-DAF-16a (342-442) fusion protein was eluted using 30 mL of buffer BD (6 M guanidine HCl, 100 mM sodium acetate, 300 mM NaCl, 10 mM imidazole, pH 4.5). The His6-SMT3-*Bm*-DAF-16a (342-442) was refolded through dialysis against 4 L of refolding buffer (20 mM Tris, 100 mM NaCl, pH 8.0) at 4°C. After 24 hours, 400 μg of His6-ubiquitin-like protease 1 (His6-Ulp-1) fusion was added to the dialysis bag, which was then transferred to a fresh 4 L of refolding buffer for an additional 24 hours of dialysis. To separate the His6-Ulp-1 and His6-SMT3 from the *Bm*-DAF-16a (342-442), the dialysate was applied to 2 mL of His60 nickel resin. The flow through and three, 10 mL buffer A washes containing Bm-DAF-16a (342-442) were collected, concentrated and buffer exchanged using ultrafiltration (MWCO 3500) into 20 mM sodium phosphate, 50 mM NaCl at either pH 6.0 or 7.4. The molecular weight of *Bm*-DAF-16a (342-442) was confirmed using a Voyager-DE Pro MALDI-TOF spectrometer (measured 11654.77 m/z, expected 11655.9 m/z).

Forkhead response element binding

Although the DNA sequence of forkhead response elements (FREs) to which *Bm*-DAF-16a binds in *B. malayi* are not known, purified *Bm*-DAF-16a (342-442) was incubated with a biotin-labeled FRE for the DAF-16 transcription factor from *C. elegans*[14] in a mobility shift assay. Mobility shift assays were performed using the Lightshift EMSA kit (Thermo

Scientific) according to manufacturer's instructions. Specifically, reactions contained 10 mM Tris pH 7.5, 50 mM KCl, 1 mM DTT, 1 μg dI/dC, 2.5% glycerol, 5 mM MgCl2, 0.05% NP-40, 5 μg purified protein and 40 fmol of biotin labeled probe. Reactions were incubated at room temperature for 20 minutes, electrophoresed at 100V on prerun 6% acrylamide in 0.5X TBE and transferred to Hybond N (GE Healthcare Life Sciences) in 0.5X TBE at 100V for 30 minutes. Detection followed manufacturer's instructions for the Lightshift EMSA kit. To generate probe, primers *Bm-daf-16*-13: 5' GATCAAGTAAACAACTATGTAAACAA 3') and *Bm-daf-16*-14 (5' GATCTTGTTTACATAGTTGTTTACTT 3') were labeled using the DNA 3' End Biotinylation Kit (Thermo Scientific). Equimolar amounts were then mixed together, heated to 95°C for 1 min and allowed to cool to room temperature for 1 hour. The same approach was used to generate a negative control probe that lacked any known FRE sequence (5' GATCCTTTGACCTAGTGACCTAGTTG 3' and 5' GATCCAACTAGGTCACTAGGTCAAAG 3').

Structure determination

All NMR measurements were acquired at 25°C at the Medical College of Wisconsin's NMR facility on a Bruker 600 MHz spectrometer equipped with a triple-resonance cryoprobe. The NMR sample consisted of 500 μM [U-^{15}N/^{13}C] *Bm*-DAF-16a (342-442), 20 mM sodium phosphate, 50 mM NaCl, 10 % D2O, 0.2 % NaN3, pH 6.0. All NMR data were processed using *NMRPipe*[15]. Standard NMR techniques were used for generating chemical shift assignments[16]. Assignments were 97.3% complete; unassigned protons are listed in Table I. Distance restraints were generated from three-dimensional ^{15}N-edited NOESY-HSQC, ^{13}C-edited NOESY-HSQC, and ^{13}C(aromatic)-edited NOESY-HSQC spectra (τmix= 80 ms). TALOS+ was used to generate backbone dihedral angle constraints[17]. The torsion-angle dynamics program *CYANA 3.0*, including the *NOEASSIGN* module, was used to calculate the *Bm*-DAF-16a (342-442) structural ensemble[18]. The 20 lowest energy conformers of 100 calculated were further refined in explicit water solvent[19]. Table I lists the structure validation statistics from the PSVS suite[20]. The structure and chemical shift assignments for *Bm*DAF-16a (342-442) were submitted to the Protein Data Bank (PDB ID 2MBF) and the Biological Magnetic Resonance Bank (BMRB ID 19398). Heteronuclear NOE spectra were obtained using the Bruker hsqcnoef3gpsi pulse program.

Characterization of the oligomeric state of Bm-*DAF-16a*

A Zorbax GF-450 column operated with 200 mM sodium phosphate at pH 7.4 at a flow rate of 1 mL per minute was used for gel filtration.

Results and Discussion

*Bm*DAF-16a (342-442) expressed as an insoluble His6-SMT3 fusion protein and was purified using immobilized metal affinity chromatography under denaturing conditions. Subsequent refolding through dialysis, incubation with His6-Ulp1, and immobilized metal affinity chromatography to remove His6-SMT3 and His6-Ulp1 isolated *Bm*DAF-16a (342-442) (Fig. S1). After concentration and buffer exchange, a two dimensional ^{15}N-^{1}H HSQC spectrum of *Bm*DAF-16a (342-442) showed a homogenous spectrum with distinct peaks throughout indicating the protein was folded (Fig. 1A). FREs in *B. malayi* are unknown, but *Bm*DAF-16a (342-442) induced a mobility shift for a canonical FRE from *C. elegans*[14], confirming folding (Fig. 1B). The solution structure of *Bm*-DAF-16a (342-442) has the characteristic fold of a forkhead box or winged helix domain containing three alpha helices (H1, H2 and H3), a short fourth alpha helix (H4) found between H2 and H3, a small three stranded antiparallel beta sheet and a C-terminal alpha helix (H5) (Fig. 1C)[12]. The ensemble of 20 lowest energy *Bm*-DAF-16a (342-442) structures shows good agreement (Fig. 1D and Fig. S2) except for the C-terminus, which heteronuclear NOE values indicate is unstructured (Fig. 1E). *Bm*DAF-16a (342-442) (11.7 Daltons) and the monomeric SMT3 (11.5 kDa) had nearly identical retention times in gel filtration suggesting that *Bm*DAF-16a (342-442) is a monomer.

At the time of submission to the PDB, *Bm*-DAF-16a (342-442) was the only forkhead box or winged helix protein from an invertebrate that we could identify in the data bank. Among forkhead box structures in the PDB, *Bm*-DAF-16a (342-442) showed the highest sequence identity to human FOXO3a, followed closely by FOXO1 and FOXO4. Obsil and Obsilova have reviewed interactions of FOXO1, FOXO3a, and FOXO4 with human FRE DNA sequences[12]. Figure 1F shows sequence alignment of *Bm*-DAF-16a and *Bm*-DAF-16b with the human FOXO domains of FOXO1, FOXO3a, and FOXO4. Residues in FOXO1, FOXO3a, and FOXO4 that bind DNA are highlighted magenta, while identical residues in *Bm*-DAF-16a/b are highlighted in cyan (Fig. 1F). Helix 3, which plays a large role in FRE interaction, has the characteristic N-X-X-R-H-X-X-S sequence (where X is any amino acid) of all forkhead box transcription factors[12]. Many of the other amino acids in FOXO1, FOXO3a, and FOXO4 that interact with DNA are identical to residues in *Bm*-DAF-16a/b. Figure 1G shows the structure of human FOXO3a bound to an FRE[21]. Figure 1H highlights the similarities to *Bm*-DAF-16a, whose residues that are identical to DNA interacting residues of FOXO1, FOXO3a, or FOXO4 are shown in cyan. Structures of FOXO3a (PDB ID 2K86)[22] and FOXO4 (PDB ID 1E17)[23] in the absence of DNA were compared to *Bm*-DAF-16a (342-442) using FATCAT[24] and were found to be substantially similar. This can be seen in the superimposition of the apo-FOXO4 structure with *Bm*-DAF-16a (342-442) (Fig. 1I) (C^{α} RMSD of 2.61 Å) along with the superimposition of FOXO3a with *Bm*-DAF-16a (342-442) (Fig. S3) (C^{α} RMSD of 3.23 Å). Most small differences between each of the structures are located in the termini or loops.

Forkhead box or FOX domains belong to different families[12]. Members of the FOXO family contain a KGDSNS insertion between H2 and H3 that is not found in other FOX families[12]. Interestingly *Bm*-DAF-16a contains a RTSQEQ insertion while the *Bm*-DAF-16b isoform contains the standard KGDSNS sequence (underlined in Fig. 1E). In the structures of human FOXO1 and FOXO3a bound to an FRE sequence, this KGDSNS insert did not bind DNA[12]. However, in the structure of human FOXO4 bound to DNA, this KGDSNS insert did interact with DNA[12]. If these insertions were to interact with DNA, similar to FOXO4, the differences in sequence may suggest a possible mechanism whereby *Bm*-DAF-16a and *Bm*-DAF-16b could distinguish between different FREs.

When the forkhead box-O domain of human FOXO3a is not bound to an FRE, it is reported to form an intramolecular interaction with conserved region three (CR3) of FOXO3a, which Wang *et al.* refers to as the closed state (Fig. 2A)[25]. Upon binding of the FOXO domain of human FOXO3a to an FRE, the displaced CR3 recognizes and binds to the KIX domain of the CREB binding protein(CBP)/p300 coactivator (Fig 2A)[25]. Figure 2A shows the model Wang *et al.* proposed for FOXO3a coativator recruitment[25]. With the exception of one residue, all CR3 interacting residues of the FOXO domain of human FOXO3a (magenta) are identical in *Bm*-DAF-16a (cyan) (Fig. 2B). Figure 2C shows the structure of human FOXO3a and Figure 2D shows the structure of *Bm*-DAF-16a (342-442). The CR3 interacting residues of FOXO3a are shown in magenta, while the identical residues in *Bm*-DAF-16a (342-442) are highlighted in cyan. The sequence alignment of *Bm*-DAF-16a/b and human FOXO1, FOXO3a, and FOXO4 identified similarities in the CR3 region of these proteins (Fig. 2E). All proteins contain the conserved φXXφφ CBP/p300 coactivator binding sequence of FOXO3a and other proteins[25,26], where φ represents any hydrophobic residue and X represents any residue. Additionally, many of the residues of the CR3 region of FOXO3a that interact with the FOXO domain of FOXO3a are identical in *Bm*-DAF-16a (Fig. 2E)[22,25].

Based on the structural similarities and sequence identities found between *Bm*-DAF-16a and human FOXO3a, we hypothesize *Bm*-DAF-16a functions as a transcription factor and recruits coactivator proteins in a fashion that is structurally similar to the model proposed by Wang *et al.* for human FOXO3a (Fig. 2A)[25]. Our method for producing *Bm*-DAF-16a, the chemical shift assignments, and the structure of *Bm*-DAF-16a (342-442) uniquely position us to experimentally test this hypothesis in future work.

Supplementary Material

Refer to Web version on PubMed Central for supplementary material.

Acknowledgments

CTV is partially supported by NIH grant 1-R15CA159202-01. University of Wisconsin-Whitewater Undergraduate Research Fellowships supported TJM, AJP, PCS and DMZ. Additional support was provided from the University of Wisconsin-Whitewater College of Letters and Sciences. The Medical College of Wisconsin provided NMR time.

References

1. Parasites - Lymphatic Filariasis. Centers for Disease Control and Prevention; 2013. http://www.cdc.gov/parasites/lymphaticfilariasis/ [accessed on 15 July 2013]
2. Pfarr KM, Debrah AY, Specht S, Hoerauf A. Filariasis and lymphoedema. Parasite immunology. 2009; 31(11):664–672. [PubMed: 19825106]
3. Ottesen EA, Hooper PJ, Bradley M, Biswas G. The global programme to eliminate lymphatic filariasis: health impact after 8 years. PLoS neglected tropical diseases. 2008; 2(10):e317. [PubMed: 18841205]
4. McCarthy J. Is anthelmintic resistance a threat to the program to eliminate lymphatic filariasis? The American journal of tropical medicine and hygiene. 2005; 73(2):232–233. [PubMed: 16103580]
5. Burglin TR, Lobos E, Blaxter ML. Caenorhabditis elegans as a model for parasitic nematodes. International journal for parasitology. 1998; 28(3):395–411. [PubMed: 9559358]
6. Riddle, DL.; Albert, PS. Genetic and Environmental Regulation of Dauer Larva Development. In: Riddle, DL.; Blumenthal, T.; Meyer, BJ.; Priess, JR., editors. C elegans II. 2. Cold Spring Harbor (NY): 1997.
7. Mukhopadhyay A, Oh SW, Tissenbaum HA. Worming pathways to and from DAF-16/FOXO. Exp Gerontol. 2006; 41(10):928–934. [PubMed: 16839734]

8. Massey HC Jr, Bhopale MK, Li X, Castelletto M, Lok JB. The fork head transcription factor FKTF-1b from Strongyloides stercoralis restores DAF-16 developmental function to mutant Caenorhabditis elegans. International journal for parasitology. 2006; 36(3):347–352. [PubMed: 16442538]
9. Gelmedin V, Brodigan T, Gao X, Krause M, Wang Z, Hawdon JM. Transgenic C. elegans dauer larvae expressing hookworm phospho null DAF-16/FoxO exit dauer. PLoS One. 2011; 6(10):e25996. [PubMed: 22016799]
10. Castelletto ML, Massey HC Jr, Lok JB. Morphogenesis of Strongyloides stercoralis infective larvae requires the DAF-16 ortholog FKTF-1. PLoS Pathog. 2009; 5(4):e1000370. [PubMed: 19360119]
11. Choi YJ, Ghedin E, Berriman M, McQuillan J, Holroyd N, Mayhew GF, Christensen BM, Michalski ML. A deep sequencing approach to comparatively analyze the transcriptome of lifecycle stages of the filarial worm, Brugia malayi. PLoS neglected tropical diseases. 2011; 5(12):e1409. [PubMed: 22180794]
12. Obsil T, Obsilova V. Structural basis for DNA recognition by FOXO proteins. Biochim Biophys Acta. 2011; 1813(11):1946–1953. [PubMed: 21146564]
13. Maiese K, Chong ZZ, Shang YC. OutFOXOing disease and disability: the therapeutic potential of targeting FoxO proteins. Trends in molecular medicine. 2008; 14(5):219–227. [PubMed: 18403263]
14. Furuyama T, Nakazawa T, Nakano I, Mori N. Identification of the differential distribution patterns of mRNAs and consensus binding sequences for mouse DAF-16 homologues. Biochem J. 2000; 349(Pt 2):629–634. [PubMed: 10880363]
15. Delaglio F, Grzesiek S, Vuister GW, Zhu G, Pfeifer J, Bax A. NMRPipe: a multidimensional spectral processing system based on UNIX pipes. J Biomol NMR. 1995; 6(3):277–293. [PubMed: 8520220]
16. Markley JL, Ulrich EL, Westler WM, Volkman BF. Macromolecular structure determination by NMR spectroscopy. Methods Biochem Anal. 2003; 44:89–113. [PubMed: 12647383]
17. Shen Y, Delaglio F, Cornilescu G, Bax A. TALOS+: a hybrid method for predicting protein backbone torsion angles from NMR chemical shifts. Journal of biomolecular NMR. 2009; 44(4): 213–223. [PubMed: 19548092]
18. Herrmann T, Guntert P, Wuthrich K. Protein NMR structure determination with automated NOE assignment using the new software CANDID and the torsion angle dynamics algorithm DYANA. J Mol Biol. 2002; 319(1):209–227. [PubMed: 12051947]
19. Linge JP, Williams MA, Spronk CA, Bonvin AM, Nilges M. Refinement of protein structures in explicit solvent. Proteins. 2003; 50(3):496–506. [PubMed: 12557191]
20. Bhattacharya A, Tejero R, Montelione GT. Evaluating protein structures determined by structural genomics consortia. Proteins. 2007; 66(4):778–795. [PubMed: 17186527]
21. Tsai KL, Sun YJ, Huang CY, Yang JY, Hung MC, Hsiao CD. Crystal structure of the human FOXO3a-DBD/DNA complex suggests the effects of post-translational modification. Nucleic acids research. 2007; 35(20):6984–6994. [PubMed: 17940099]
22. Wang F, Marshall CB, Yamamoto K, Li GY, Plevin MJ, You H, Mak TW, Ikura M. Biochemical and structural characterization of an intramolecular interaction in FOXO3a and its binding with p53. J Mol Biol. 2008; 384(3):590–603. [PubMed: 18824006]
23. Weigelt J, Climent I, Dahlman-Wright K, Wikstrom M. Solution structure of the DNA binding domain of the human forkhead transcription factor AFX (FOXO4). Biochemistry. 2001; 40(20): 5861–5869. [PubMed: 11352721]
24. Ye Y, Godzik A. Flexible structure alignment by chaining aligned fragment pairs allowing twists. Bioinformatics. 2003; 19(suppl 2):ii246–ii255. [PubMed: 14534198]
25. Wang F, Marshall CB, Li GY, Yamamoto K, Mak TW, Ikura M. Synergistic interplay between promoter recognition and CBP/p300 coactivator recruitment by FOXO3a. ACS Chem Biol. 2009; 4(12):1017–1027. [PubMed: 19821614]
26. Wang F, Marshall CB, Yamamoto K, Li GY, Gasmi-Seabrook GM, Okada H, Mak TW, Ikura M. Structures of KIX domain of CBP in complex with two FOXO3a transactivation domains reveal

promiscuity and plasticity in coactivator recruitment. Proc Natl Acad Sci U S A. 2012; 109(16): 6078–6083. [PubMed: 22474372]

27. Brunger, AT. A system for X-ray crystallography and NMR. New Haven: CT Yale University Press; 1992. X-PLOR, version 3.1.
28. Engh RA, Huber R. Accurate bond and angle parameters for X-ray protein structure refinement. Acta Crystallographica Section A. 1991; 47(4):392–400.
29. Schwieters CD, Kuszewski JJ, Tjandra N, Marius Clore G. The Xplor-NIH NMR molecular structure determination package. J Magn Reson. 2003; 160(1):65–73. [PubMed: 12565051]
30. Laskowski RA, Rullmannn JA, MacArthur MW, Kaptein R, Thornton JM. AQUA and PROCHECK-NMR: programs for checking the quality of protein structures solved by NMR. J Biomol NMR. 1996; 8(4):477–486. [PubMed: 9008363]

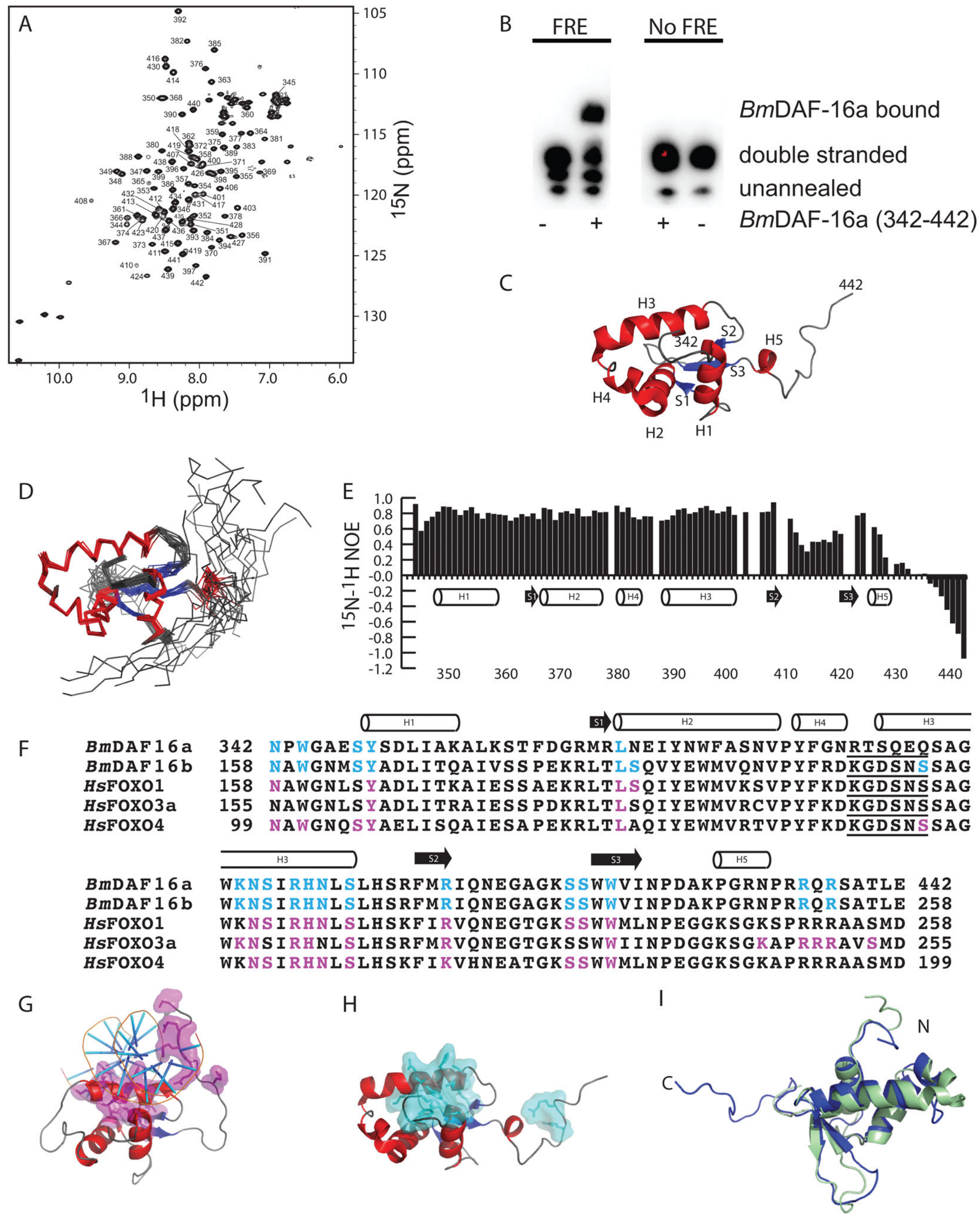

Figure 1. Residues in *Bm*DAF-16a (342-442) are identical to FRE interacting residues in human FOXO proteins

A) ^{15}N-^{1}H HSQC spectra of 500 μM [U-^{15}N/^{13}C] *Bm*DAF-16a (342-442) with backbone amide assignments. B) Mobility shift assay showing *Bm*-DAF-16a (342-442) binds to DNA containing a canonical FRE sequence from *C. elegans* and does not bind DNA lacking an FRE sequence. C) The lowest energy structure of *Bm*DAF-16a (342-442). D) Ensemble of 20 *Bm*DAF-16a (342-442) structures. E) ^{15}N-^{1}H heteronuclear NOE values plotted versus *Bm*DAF-16a (342-442) residue. F) Sequence alignment of *Bm*DAF-16a and *Bm*DAF-16b with the DNA binding domains of human FOXO1, FOXO3a, and FOXO4. FRE interacting residues in human FOXO1, FOXO3a, and FOXO4 are highlighted magenta[12]. Residues in *Bm*DAF-16a and *Bm*DAF-16b that are identical to DNA interacting residues of the human FOXO proteins are highlighted in cyan. The five amino acid insert consistent with FOXO domains, but not other FOX family members, is underlined[12]. G) Human FOXO3a bound to an FRE (PDB ID 2UZK)[21]. DNA interacting residues of FOXO3a are shown in magenta. H) Solution structure of *Bm*DAF-16a (342-442) with residues identical to DNA interacting residues from human FOXO proteins shown in cyan. I) Superimposition of the *Bm*-DAF-16a (342-442) (blue) and FOXO4 (green, PDB ID 1E17).

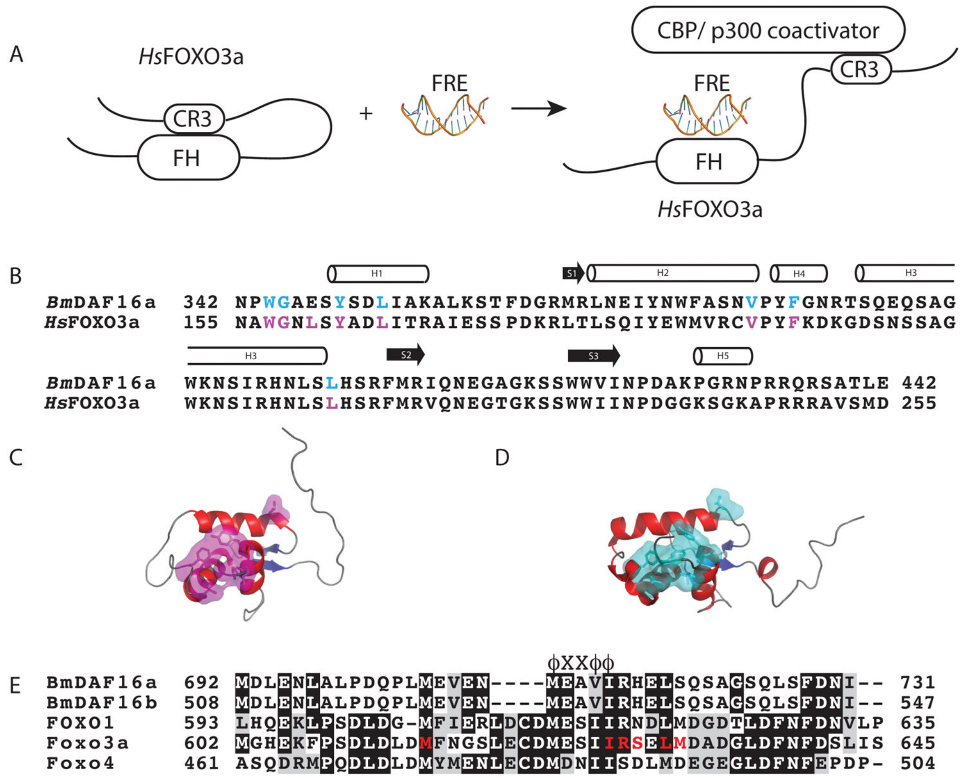

Figure 2. Similarities between the structures and identities in the sequences of *Bm*DAF-16a (342-442) and human FOXO3a suggest a potential similarity in coactivator recruitment

A) Mechanism of human FOXO3a recruitment of coactivator proteins proposed by Wang *et al.*[25]. In the absence of an FRE, human FOXO3a adopts a closed state where the DNA binding domain forms an intramolecular interaction with conserved region three (CR3)[25]. Binding to an FRE displaces CR3 and allows for recruitment of CREB binding protein (CBP) or p300 coactivator through the interaction with CR3[25]. B) Sequence alignment of *Bm*DAF-16a (342-442) with human FOXO3a. CR3 binding residues in human FOXO3a are shown in magenta while identical residues in *Bm*DAF-16a (342-442) are shown in cyan. C) Crystal structure of human FOXO3a (PDB ID 2UZK) with CR3 binding residues highlighted in magenta. D) Solution structure of *Bm*DAF-16a (342-442) with residues identical to CR3 interacting residues from human FOXO3a. E) Sequence alignment of the CR3 region of *Bm*-DAF16a/b and human FOXO1, FOXO3a and FOXO4. FOXO3a CR3 residues that are reported to interact with the forkhead DNA binding domain are colored red[22]. The φXXφφ label, where φ represents any hydrophobic residue and X represents any residue, identifies the conserved CBP/p300 coactivator binding sequence of FOXO3a[25].

Table I

Structure statistics for 20 *Bm*DAF-16a conformers (PDB ID 2MBF, BMRB ID 19398).

Completeness of resonance assignments (%) [a]		97.3%
Constraints		
Non-redundant distance constraints		
Total		2954
Intraresidue [i=j]		1771
Sequential [(i−j)=1]		455
Medium [1<(i−j)≤5]		415
Long		313
Dihedral angle constraints (φ and ψ)		114
Constraints per residue		
Average number of constraints per residue		30
Constraint Violations		
Average number of distance constraint violations per structure		
0.1–0.2 Å		18.15
0.2–0.5 Å		1.85
> 0.5 Å		0
Average R.M.S. distance violation per constraint (Å)		0.02
Maximum distance violation (Å)		0.36
Average number of dihedral angle violations per structure		
1–10°		9.55
> 10°		0
R.M.S. dihedral angle violation per constraint (°)		0.62
Maximum dihedral angle violation (Å)		4.9
Average atomic R.M.S.D. to the mean structure (Å)		
Residues 342–406		
Backbone (Cα, C′, N)		0.42 ± 0.07
Heavy atoms		0.89 ± 0.09
Deviations from idealized covalent geometry [b]		
Bond lengths	R.M.S.D. (Å)	0.015
Torsion angle violations	R.M.S.D. (°)	1.2
Lennard-Jones energy [c] (kJ mol^{-1})		−2180 ± 80
Ramachandran statistics (% of all residues) [d]		
Most favored		95.1
Additionally allowed		4.9

Generously allowed	0.1
Disallowed	0

[a]Missing chemical shifts include: H of Asn342; Hζ of Phe 374; Hα and Qβ of Ser 386; H of Gln 387; Hδ1 and Hε1 of His 399; H, Hδ1 and Hε1 of His 400; H of Ser 405; Hε3 and Hζ3 of Trp 420; and H of Trp 421.

[b]Final X-PLOR[27] force constants were 250 (bonds), 250 (angles), 300 (impropers), 100 (chirality) and 100 (omega), 50 (NOE constraints), and 200 (torsion angle constraints). Idealized covalent geometry is from Engh and Huber[28].

[c]Nonbonded energy was calculated in XPLOR-NIH[29].

[d]Values are from PROCHECK-NMR[30]